THE ASTROPHYSICAL JOURNAL, 286:171–185, 1984 November 1

AN ANALYSIS OF THE NARROW-LINE PROFILES IN HIGH IONIZATION SEYFERT GALAXIES[1]

M. M. DE ROBERTIS AND D. E. OSTERBROCK
Lick Observatory, Board of Studies in Astronomy and Astrophysics, University of California, Santa Cruz
Received 1984 April 6; accepted 1984 May 21

ABSTRACT

Narrow optical emission-line profiles representing a wide range in ionization potential for 12 high-ionization Seyfert galaxies are analyzed using deconvolution techniques. The data reduction process is described in detail. A good correlation is found between line width and ionization potential in many of the objects. For some galaxies a good correlation is also found between line width and critical density. For a given object, the ratios of line widths at various fractions of full intensity are remarkably similar over the entire range of ionization potential and critical density. Almost identical velocity ratios at corresponding fractions of maximum intensity are found for profiles from an individual line (e.g., [Fe VII] λ6087) taken from every object. In particular the relation between the velocity widths at $\frac{1}{2}$ and $\frac{1}{4}$ maximum intensity is the same found for the widths of the broad profiles of Hβ in Seyfert 1 galaxies and QSOs by De Robertis (1984*a*). This may suggest that a similar acceleration mechanism (and/or geometry) operates in all objects in both the broad- and narrow-line regions.

The high-ionization line widths correlate only poorly with the absolute blue magnitude of the galaxy, while the lower ionization lines show a good correlation. On average, half of the galaxies have narrow line profiles which are skewed to the blue, half which are symmetric. The low-ionization lines display little asymmetry in general, while the high-ionization lines tend to have blueward excesses.

The possible implication of these and other correlations, and the absence of still other correlations, are discussed. Descriptions of the details of the individual spectra are presented.

Subject headings: galaxies: Seyfert — line profiles

I. INTRODUCTION

It has long been suggested that the broad lines in the spectra of Seyfert 1 nuclei arise in relatively dense gas ($\sim 10^{8-10}$ cm^{-3}) close to the source of photoionization (≤ 1 pc) with a relatively large velocity dispersion, while the narrow lines come from separate, less dense regions ($\sim 10^{3-6}$ cm^{-3}) with considerably smaller dispersions at much greater distances ($\sim 10^2$ pc). (See, for example, Osterbrock 1978*a*; Davidson and Netzer 1979). The narrow-line region (NLR) has been resolved in some of the nearest Seyfert galaxies (e.g., NGC 1068 by Walker 1968). Spectrophotometric measurements seem to show that the narrow-line fluxes, especially [O III] $\lambda\lambda$ 4959, 5007, do not change on month-year time scales, as the broad-line fluxes can. They therefore tend to suggest that the narrow-line dimensions are much greater than the broad-line region scales.

There is also some evidence that within the broad-line region (BLR) itself, the high-ionization lines like He II λ4686 are broader than the low-ionization lines like the Balmer lines. For high-ionization objects it has also been observed that the very high ionization lines, especially those of [Fe VII], [Fe X], [Fe XI], and even [Fe XIV], have full widths at half-maximum (FWHM) which, while not as large as the bona fide broad profiles, are certainly broader that the typical low-ionization lines such as [O I] or [N I] (see, for example, Wilson 1979; Osterbrock 1981; Whittle 1982).

Over the past 10 years, Osterbrock and various collaborators have obtained spectra of many active galactic nuclei using the image-dissector scanner (IDS) (Robinson and Wampler 1972; Miller, Robinson, and Wampler 1976; Miller, Robinson, and Schmidt 1980) with the Shane 3 m telescope of Lick Observatory. These data were taken principally at two resolutions: with a grating of 600 lines mm^{-1}, covering about 2560 Å at an instrumental resolution with FWHM $\approx$ 10 Å, and a grating with 1200 lines mm^{-1}, covering 1280 Å per scan with an instrumental profile with FWHM $\approx$ 5 Å. We have selected from these data high-quality spectra of 12 high-ionization Seyfert galaxies—from the ultraviolet to the near infrared—in order to study the emission-line profiles covering a very large range in ionization potential. All of them are Seyfert 1 or Seyfert 1.5 galaxies, except for Mrk 533, usually classified as a Seyfert 2 with noticeably asymmetric emission-line profiles (Shuder and Osterbrock 1981). In all these galaxies, the narrowest lines have FWHMs only marginally larger than the narrowest lines of the corresponding comparison lamps (which are assumed to be representative of the instrumental profile). In order to study both qualitatively and quantitatively all the narrow-line profiles, it is necessary to remove such instrumental effects as fully as possible.

The relatively high signal-to-noise of the IDS data (>30 in the continuum and up to 250 in strong emission lines) and sufficient oversampling by the IDS (by a factor of 7–8 for the particular configuration used) suggest that Fourier deconvolution techniques may be useful here. The following section describes the reduction procedure applied to all of the spectral scans.

II. DATA REDUCTION

a) Procedure

For each of the objects we selected the highest resolution, highest signal-to-noise scan for a given wavelength coverage, along with the corresponding lamp exposure for the deconvol-

[1] *Lick Observatory Bulletin* No. 983.

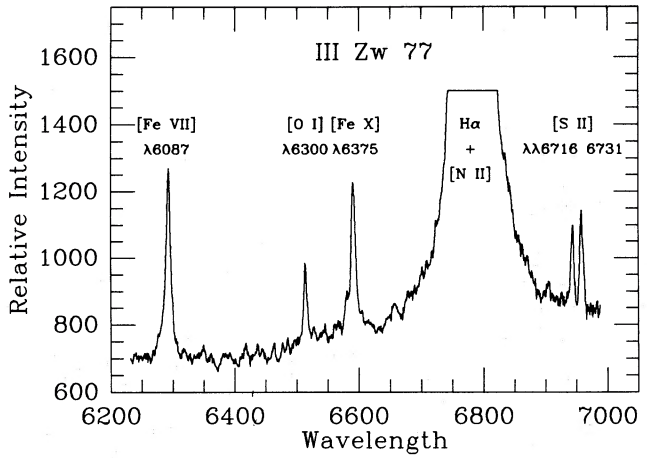

FIG. 1a

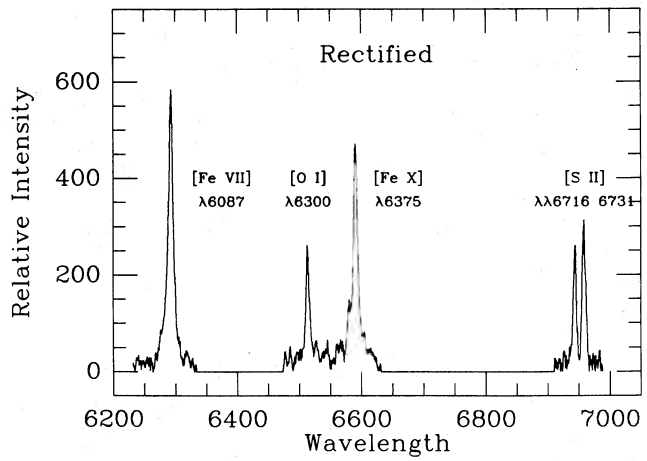

FIG. 1b

FIG. 1.—(*a*) Section of observed spectral scan of III Zw 77. In this as in all scans in this papers the relative intensity is given in energy flux units per unit wavelength interval as a function of wavelength in the rest system of the Sun. (*b*) Same section of same scan rectified as described in text.

ution procedure. Scans were summed only if taken in the same night with the same configuration, since the instrumental profiles can vary enough between successive nights to cause an artificial smoothing of the profiles if summed. Figure 1 shows an example of a section of an IDS scan (in energy units per unit wavelength interval) of the red region of III Zw 77 at an effective resolution of 5 Å. (The relatively strong Hα profile has been truncated for this illustration.) This scan is representative of the "average" signal-to-noise in most of the data. Notice that the effective signal-to-noise ratio, as far as deconvolution techniques are concerned, is actually less than the "true" ratio since the continua of Seyfert galaxies can contain stellar features (e.g., weak absorption lines). In each portion of the data spectrum all the "available" narrow lines were first identified, and the spectrum was then rectified using an interactive spline fit to the continuum. The interline regions were set to zero at the same time. Almost all phases in the data reduction were carried out using RETICENT, a one-dimensional spectrophotometric command language (Pritchet, Mochnacki, and Yang 1982). Figure 1*b* shows the results of this phase of the reduction on the data of Figure 1*a*. It is the somewhat subjective nature of the continuum fitting procedure that introduces the largest uncertainty in the profile widths. While we can never be sure that the adopted fit is "perfect," a consistent approach was used for the same spectral region in each object throughout. In principle, one might check the continuum fit by comparing the measured line ratios from transitions from the same upper level in a particular atom to the theoretical (transition probability) ratios [e.g., I([O III] λ4959)/I([O III] λ5007), I([Fe VII] λ5721)/I([Fe VII] λ6087), or I([Ne V] λ3346)/I([Ne V] λ3426)] if they were exactly known. In practice, however, we find that one or both of the components can sometimes be blended with other (weaker) lines. The [O III] ratios were always very nearly 2.9, as expected. In the cases where blending did not appear too serious, the [Ne V] ratios were nearly as expected, i.e., 2.7. The [Fe VII] ratios were more difficult to measure and often were blended in the wings making estimates uncertain.

In order to reduce considerably the high-frequency component in the data transform, the far wings of each of the narrow lines (unless they were blended) were tapered smoothly to the adopted continuum (from the level of a few percent of the line maximum) by redefining the far wings using interactive spline fits. Comparing Figures 1*b* and 2 (the spline-tapered profiles) indicates that the effective noise in the far wings and continuum has been reduced considerably without affecting the bulk of the emission line profile.

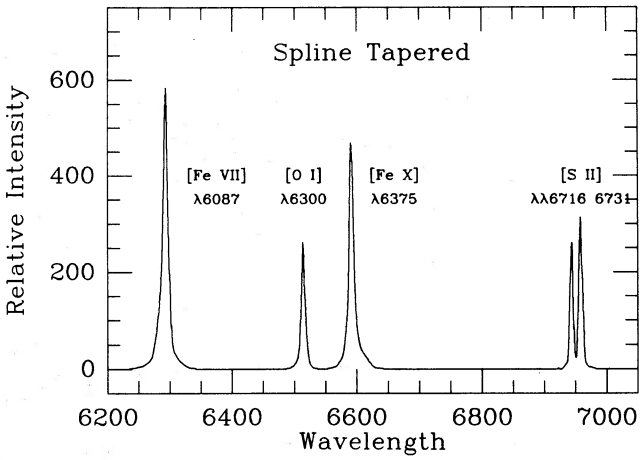

FIG. 2a

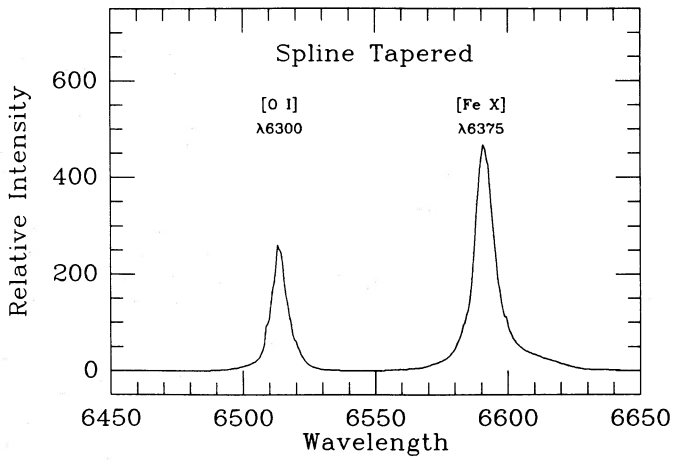

FIG. 2b

FIG. 2.—(*a*) Same section of scan of III Zw 77, with wings of lines smoothed by spline tapering, as described in text. (*b*) Enlarged section of same spline tapered scan, showing [O I] λ6300 and [Fe X] λ6375 at large wavelength scale.

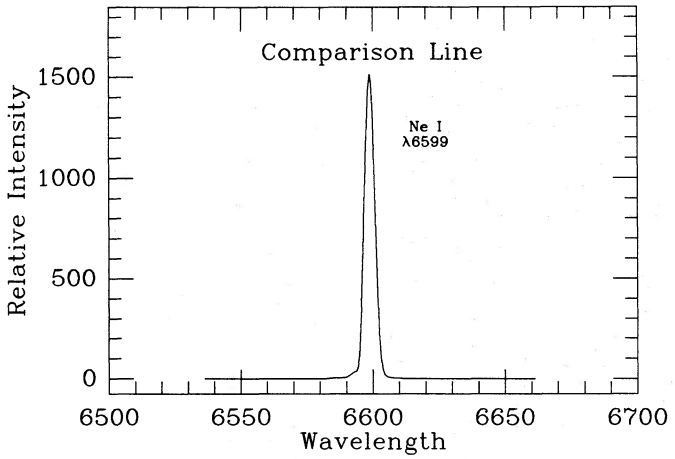

FIG. 3*a*

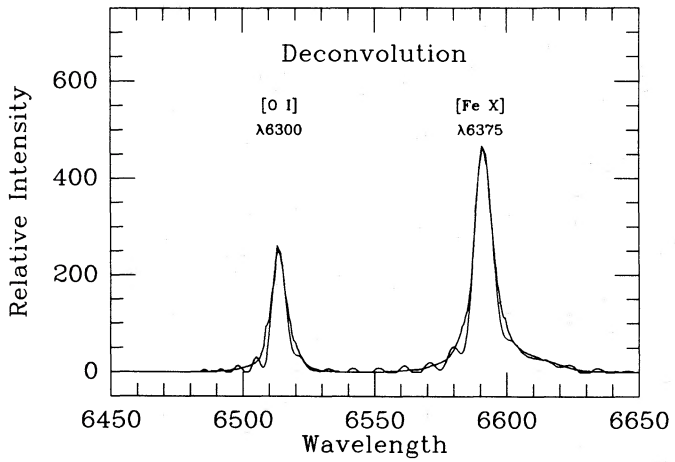

FIG. 3*b*

FIG. 3.—(*a*) Ne I λ6599 comparison line used for instrumental profile. (*b*) Deconvolved profiles of [O I] λ6300 and [Fe X] λ6375 from III Zw 77 scan.

To isolate the instrumental profile, all the strong, unblended comparison lines from the appropriate lamp were analyzed with a specifically developed routine in RETICENT. The full widths at $\frac{3}{4}$, $\frac{1}{2}$, $\frac{1}{3}$, $\frac{1}{4}$, and $\frac{1}{5}$ of maximum intensity were recorded for each of the lines as well as the asymmetries at each position. (Asymmetry at a given intensity here refers to the difference between the centroid at the intensity and the centroid at $\frac{1}{2}$ maximum intensity. A quantitative definition is provided below. It is used as an indicator of the skewness of the profiles.) Usually the comparison profiles within the region of interest in each scan were similar enough to be considered the same. If there seemed to be systematic change across the region, then an appropriate number of lines were selected as "instrumental" profiles, depending on the wavelength of the galaxy lines. For consistency, all lines were treated in the same manner regardless of how broad they may have been originally, compared with the instrumental profile. Figure 3*a* shows, on the same scale as the tapered profiles, the instrumental profile (Ne I λ6599 from the lamp) adopted for the region of the spectrum under discussion. The signal-to-noise ratio in the comparison lamp (and line) is much higher than in the data.

The Fourier transform and inverse transform programs used in the subsequent deconvolution analysis are contained in the program SPROC written by A. Hatzes at Lick Observatory. Careful tests were made prior to the analysis, to ensure that the transforms operated reliably using specific examples. In particular, analysis of deconvolved real data profiles which were initially many times broader than the instrumental profile showed that the widths and asymmetries remained, at an accuracy substantially better than the accuracy we quote for the procedure below.

The measured parameters for this line and the instrumental line of Figure 3*a* are listed in Table 1. Also listed are the parameters for the adopted deconvolved profiles of [O I] λ6300, and [Fe X] λ6375, which are shown in Figure 3*b* (on the same scale as the previous figure) in comparison with the "before" profiles of Figure 2*b*. We note that the asymmetries indicated by the "before" profiles are qualitatively preserved. "Ringing" in the wings of the profiles is clearly evident, but such effects do not seriously degrade line width estimates above about 20% of the maximum intensity in the line. Hence, width and asymmetry estimates will be given down to this level. The largest source of error for measurements of weak lines such as those in Figures 2*b* and 3*b* is introduced chiefly by the placement of the continuum. This will be discussed below.

b) Deconvolution theory

Denote the input (data) spectrum or profile $O(\lambda)$, and the relevant comparison line profile $I(\lambda)$. The Fourier transform of

TABLE 1

LINE WIDTHS AND ASYMMETRIES

Line ID	$v_{1/2}$ (km s^{-1})	$v_{1/3}$ (km s^{-1})	$v_{1/4}$ (km s^{-1})	$v_{1/5}$ (km s^{-1})	$a_{1/3}$	$a_{1/4}$	$a_{1/5}$
Ne I λ6599 comparison line	205	260	285	300	−0.011	−0.019	−0.026
[a][O I] λ6300: original profile	305	450	510	575	−0.036	−0.003	−0.037
[b][O I] λ6300: deconvolved profile	280	350	390	425	−0.014	−0.025	−0.035
[b][Fe X] λ6375: original profile	385	515	640	765	−0.025	−0.018	−0.019
[Fe X] λ6375: deconvolved profile	370	470	530	585	−0.013	−0.023	−0.034

[a] At λ6514 in the observed frame.
[b] At λ6592 in the observed frame.

a profile will be represented by the subscript F. Ideally the "true" line profile will be the convolution,

$$O(\lambda) = \int_0^\infty T(\lambda - x)I(x)dx \,, \quad (1)$$

or in frequency space a multiplication,

$$O_F(k) = T_F I_F \,. \quad (2)$$

The real data, however, have a finite signal-to-noise which renders the deconvolved profile very noisy and in general unacceptable for analysis. An optimum (Wiener) filter substantially reduces the amplitude of the unwanted high-frequency components (e.g., Brault and White 1971). The Fourier transform of the optimum filter F_F is

$$F_F(k) = \frac{S(k)}{S(k) + N(k)} \,, \quad (3)$$

where S is the Fourier transform of the ideal observed line profile, and N is the transform of the noise spectrum. The ratio of the amplitudes is just the signal-to-noise of the observations. The transform of the "true" profile becomes

$$O_F(k) = T_F(k)I_F(k)F_F(k) \,. \quad (4)$$

In our case, the noise is assumed to be random or white noise (frequency independent). For S we adopt a Gaussian with the appropriate FWHM because not only is the observed profile roughly Gaussian (especially in the core) but, more importantly, it turns out from our experiments that the resulting "true" profiles are not very sensitive to the analytic form that is adopted for S. We emphasize again that the largest source of error in the true profile is the uncertainty in the adopted continuum placement which isolates the data line. In practice, the signal-to-noise was estimated from the data, and small adjustments to this figure were made in the deconvolution process to minimize the signal-to-noise in the continuum in the final profile. The profiles in each scan were analyzed individually where possible. The deconvolved "after" profiles, and the original "before" data profiles were analyzed with the same RETICENT routine mentioned above for the purposes of comparison. For the narrowest lines, the deconvolved profiles were narrower at all heights than the original observed profiles, with the FWHMs related approximately as one would expect using the naive "quadrature" technique in most cases. Because the narrowest profiles had essentially instrumental widths above half-maximum, and noise in the final spectrum may affect the lower 15% of the profile, the profiles were analyzed and recorded only between $\frac{1}{2}$ and $\frac{1}{5}$ maximum. Asymmetries noted in the original profiles were preserved in the final data for the most part, except in isolated cases where the data and the comparison lines were asymmetric in the same sense, and the true profile was approximately symmetric.

III. RESULTS

Table 2 lists the lines identified and measured in at least some of the objects. The lines are identified by element and stage of ionization, and include the wavelength (Å), the ionization potential (eV) of the previous stage of ionization to the stage which produces the observed lines, and the critical density of the term (cm^{-3}) at 10^4 K. The critical density is

TABLE 2

IONIZATION POTENTIALS AND CRITICAL DENSITIES

Stage of Ionization	Wavelength (Å)	Ionization Potential (eV)	Critical Density (cm^{-3})
Ne V	3346	97.1	1.6E + 07
Ne V	3426	97.1	1.6E + 07
Fe VII	3588	99.1	3.7E + 07
O II	3727	13.6	4.5E + 03
Fe VII	3760	99.1	3.7E + 07
Fe V	3840	54.8	(1.1E + 07)
Ne III	3869	41.0	9.7E + 06
Fe V	3893	54.8	...
Ne III	3968	41.0	9.7E + 06
S II	4068	10.4	6.9E + 06
Fe V	4071	54.8	(5.7E + 07)
O III	4363	35.1	3.3E + 07
He II	4688	54.9	...
H I	4861	13.6	...
O III	4959	35.1	7.0E + 05
O III	5007	35.1	7.0E + 05
Fe VI	5146	75.0	2.7E + 07
Fe VII	5159	99.1	3.3E + 06
Fe VI	5176	75.0	3.3E + 07
N I	5199	0.0	2.0E + 03
Fe XIV	5303	361.0	...
Fe VII	5721	99.1	3.6E + 07
Fe VII	6087	99.1	3.6E + 07
O I	6300	0.0	1.8E + 06
S III	6312	23.3	1.4E + 07
Fe X	6375	233.6	...
S II	6716	10.4	1.5E + 03
S II	6731	10.4	3.9E + 03
Ar III	7135	27.6	4.8E + 06
Fe XI	7892	262.1	...

defined as the density at which the collision rate is equal to the radiative deexcitation rate:

$$N_{cr} = \frac{\Sigma_{j<i} A_{ij}}{\Sigma_{j<i} q_{ij}} \,, \quad (5)$$

where A_{ij} is the radiative transition rate from level i to j, and $N_e q_{ij}$ is the collisional transition rate. Transitions to different levels within the same term have been omitted from numerator and denominator. For the [Fe VII] lines, the rates were taken from Nussbaumer and Storey (1982), while all other critical densities were based on numerical values collected by Mendoza (1983). For H I, He I, and He II, $N_{cr} \gg 10^9$ cm^{-3}. For [Fe V], calculated collision strengths are not available. Therefore the approximate critical densities listed in parentheses in Table 2 are based on approximate collision strengths estimated by analogy with the [Fe VI] and [Fe VII] calculations of Nussbaumer and Storey (1978, 1982), and on transition probabilities calculated by Garstang (1957). Unfortunately, [Fe V] λ3893 is a blend of $^5D_4$–$^3F_4$ λ3891.3 and $^5D_3$–$^3P_2$ λ3895.5 (Bowen 1960) and cannot be directly compared with the other single lines.

Table 3 contains the name of each high-ionization galaxy, the emission-line redshift, the apparent blue magnitude of the galaxy m_B, and the velocity width of the broad component of Hβ at half-maximum $v_{1/2}$(Hβ). All the spectra used in this investigation were taken in the years 1975–1981. The redshifts (in the rest system of the Sun) are from Huchra (1983) and are identical to measurements from our scans to at least three significant figures. The m_B values are also from Huchra (1983). For the Markarian and Arakelian galaxies, they are identical to the values given in the respective discovery papers. In themselves these values are probably only accurate to ± 0.5 mag.

TABLE 3

SEYFERT GALAXIES OBSERVED

Galaxy Name	Redshift z	m_B	$v_{1/2}(H\beta)$ (km s^{-1})
NGC 4051	0.0020	11.5	990
NGC 4151	0.0032	11.2	7930
III Zw 77	0.0350	15.4	890
Mrk 9	0.0397	15.0	3200
Mrk 359	0.0167	15.5	430
Mrk 533	0.0289	16.0	480
Mrk 704	0.0293	15.2	6170
Mrk 975	0.0492	15.0	2350
Mrk 1040	0.0155	15.0	2180
Mrk 1126	0.0104	14.5	2620
Mrk 1239	0.0199	14.5	1150
Akn 564	0.0246	14.4	820

Even though all the candidate objects but one are Seyfert 1 galaxies, large-aperture, broad-band measurements are likely to contain substantial contributions from the galaxy as well as the nucleus. The velocity widths of broad Hβ were estimated from the appropriate scans. In cases where the narrow/broad dichotomy was not obvious, NGC 4051, III Zw 77, Mrk 359, Mrk 533, Mrk 1040, Mrk 1239, and Akn 564, the width listed is for the entire Hβ profile.

Table 4 summarizes the results of our measurements for each galaxy. Column (1) gives the wavelength of the line for which columns (2)–(5) list the full width at $\frac{1}{2}$, $\frac{1}{3}$, $\frac{1}{4}$, and $\frac{1}{5}$ maximum (km s^{-1}), and columns (6)–(9) give the asymmetry parameters at $\frac{1}{3}$, $\frac{1}{4}$, and $\frac{1}{5}$ maximum. The dimensionless asymmetry parameter a at relative intensity h, a_h, is defined as the difference in the centroid at h, λ_h, and the centroid at $\frac{1}{2}$ maximum $\lambda_{1/2}$, normalized by the width of the line at relative intensity h, $\Delta\lambda_h$, i.e.,

$$a_h = \frac{\lambda_{1/2} - \lambda_h}{\Delta\lambda_h} . \quad (6)$$

Estimates of the errors associated with the velocities depend on the relative intensity of the line since continuum fitting introduces the largest uncertainty. The error in the strongest lines is at most 5%, while for the weakest lines, errors of over 10% are possible.

Note that [O II] λ3727 is actually a close, unresolved doublet, $\lambda\lambda$3726, 3729, which we have treated as a single line. The individual components are therefore actually slightly narrower than the values quoted in the table. The maximum effect (for equal strengths of the two components) is an overestimate of the [O II] widths by 220 km s^{-1}. All the correlations we have found would be slightly improved by any correction for this effect.

The data were analyzed in two phases: (I) by individual galaxy to determine how lines compare over a wide range of ionization, and (II) by individual line to determine how lines vary from galaxy to galaxy. Possible linear correlations between each set of measurements were investigated using a least-squares routine. We report below only the cases where some correlation was found between variables.

I. There is a good correlation between the line widths and the ionization potentials for many of the candidate objects. (The linear correlation coefficient, R, ranges between 0.5 and 0.8 for about half of the galaxies.) Two of the best correlations were found for Akn 564, and Mrk 1040, viz.,

$$v_{1/3} = 3.5(\pm 0.7)\mathrm{IP} + 310(\pm 70) \quad \text{(Akn 564)} ,$$
$$v_{1/3} = 2.5(\pm 0.8)\mathrm{IP} + 490(\pm 70) \quad \text{(Mrk 1040)} , \quad (7)$$

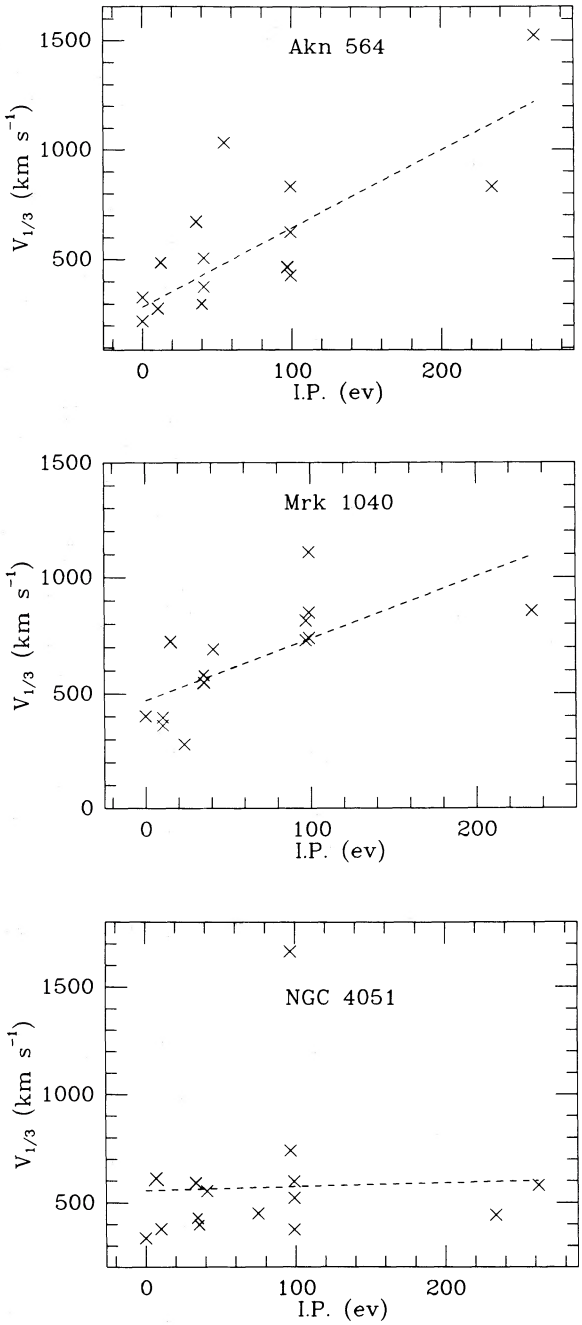

FIG. 4.—Correlations of emission-line widths (at one-third maximum intensity) with ionization potential (as defined in text) for three Seyfert 1 galaxies.

where $v_{1/3}$ is the velocity width (km s^{-1}) at $\frac{1}{3}$ maximum of the profile of a line with ionization potential IP (eV), and the formal errors associated with the variables are given in brackets. These correlations are illustrated in Figure 4*a*, *b*. For the objects in which a definite correlation was detected, the slopes varied between 1.3 and 6.6, whereas the intercepts (widths for lines with zero ionization potential) ranged between 71 and 156 km s^{-1}. The differences in the slopes appear to be real, and if so, reflect real differences in the ionization/velocity structure in the different NLRs. That is, a given ionization zone may sample different portions of the velocity field in different objects. On the other hand, there does not appear to be any

TABLE 4

SUMMARY OF LINE WIDTHS AND ASYMMETRIES

Lambda (Å)	$v_{1/2}$	$v_{1/3}$	$v_{1/4}$ (km s^{-1})	$v_{1/5}$	$a_{1/3}$	$a_{1/4}$	$a_{1/5}$
			NGC 4051				
3346	1330	1660	1830	1940	-0.028	-0.037	-0.042
3426	600	730	800	840	0.000	0.001	0.001
3727	590	650	800	840	-0.005	-0.006	-0.008
3760	420	520	560	590	-0.001	-0.002	-0.001
3869	450	550	600	630	-0.003	-0.005	-0.004
4363	470	590	650	700	0.010	0.018	0.025
4959	350	420	460	480	0.003	0.001	0.000
5007	330	400	430	460	-0.001	-0.001	-0.001
5159	480	590	650	700	0.015	0.025	0.033
5176	360	450	490	520	0.014	0.021	0.026
6087	300	370	410	440	0.002	0.005	0.006
6300	270	330	360	380	-0.011	-0.015	-0.019
6375	350	440	490	520	0.003	0.006	0.008
6716	300	370	410	440	0.001	0.002	0.002
7892	460	580	650	710	0.011	0.025	0.043
			NGC 4151				
3346	1220	1490	1630	1730	0.009	0.014	0.017
3426	1170	1450	1600	1710	-0.003	-0.006	-0.007
3727	800	980	1070	1140	0.003	0.003	0.004
3869	780	960	1050	1110	-0.014	-0.021	-0.026
3968	570	730	820	900	-0.006	-0.012	-0.019
4068	610	760	850	920	-0.004	-0.011	-0.015
4363	850	1170	1370	1510	0.073	0.106	0.124
4686	380	490	550	590	-0.015	-0.025	-0.028
4861	510	650	730	800	-0.005	-0.010	-0.014
4959	440	560	630	680	0.009	0.015	0.021
5007	470	600	670	740	0.001	0.020	0.030
5199	500	640	720	780	0.025	0.041	0.053
6087	570	790	890	950	0.067	0.080	0.083
6300	470	600	690	760	0.000	0.000	-0.004
6716	430	550	620	670	0.011	0.014	0.013
6731	430	550	620	660	0.013	0.015	0.014
7513	670	860	980	1110	-0.012	-0.024	-0.043
7325	950	1200	1350	1460	0.005	0.008	0.012
			III ZW 77				
3346	450	570	640	700	0.006	0.008	0.011
3426	400	500	560	600	0.002	0.001	0.002
3588	520	680	800	960	0.027	0.059	0.105
3727	460	580	640	690	0.008	0.014	0.020
3760	410	520	590	680	0.017	0.031	0.064
3869	290	370	410	450	0.014	0.024	0.036
3968	430	540	620	680	-0.017	-0.030	-0.046
4363	460	580	650	700	-0.001	-0.001	0.001
4959	300	370	410	440	0.013	0.022	0.028
5007	280	350	390	420	0.007	0.011	0.013
5176	330	400	440	460	0.001	0.001	0.002
5303	450	-	-	-	-	-	-
5721	290	360	400	420	0.002	0.002	0.006
6087	420	490	540	570	-0.016	-0.025	-0.034
6300	200	250	280	300	0.007	0.012	0.017
6375	320	410	460	510	-0.012	-0.024	-0.037
6716	230	280	310	330	-0.017	-0.026	-0.032
6731	270	340	370	390	-0.013	-0.021	-0.028
7892	230	290	340	500	0.019	0.058	0.168
			MRK 9				
3426	1270	1580	1760	1890	0.002	0.004	0.005
3727	1090	1380	1550	1680	0.026	0.041	0.055
3760	1530	1880	2050	2170	-0.036	-0.048	-0.056
4363	1230	1800	2080	2240	-0.085	-0.105	-0.108
4959	430	520	570	600	0.001	0.004	0.006
5007	430	530	590	620	0.013	0.018	0.023
5721	1300	1600	1870	2050	-0.005	-0.011	-0.018
6087	940	1200	1340	1440	0.028	0.042	0.051
6300	1210	1590	1740	1850	0.049	0.056	0.059
6716	230	300	340	400	0.004	0.007	0.005
6731	250	320	370	400	-0.006	-0.007	-0.007
7892	910	1230	1430	1560	0.058	0.082	0.094

TABLE 4—*Continued*

Lambda (Å)	$v_{1/2}$	$v_{1/3}$	$v_{1/4}$	$v_{1/5}$	$a_{1/3}$	$a_{1/4}$	$a_{1/5}$
		(km s^{-1})					
			MRK 359				
3426	370	460	500	530	0.003	0.004	0.005
3727	470	580	640	680	-0.011	-0.028	-0.032
3869	270	330	350	370	-0.001	-0.001	-0.013
4363	590	710	780	820	-0.008	-0.014	-0.016
4686	350	430	470	500	0.003	0.004	0.005
4959	210	250	270	290	-0.012	-0.016	-0.018
5007	190	230	260	270	0.002	0.004	0.007
5159	210	270	320	350	0.027	0.052	0.070
5176	210	250	280	290	-0.001	-0.004	-0.005
5199	260	310	340	360	-0.002	-0.004	-0.006
5305	540	660	730	770	0.011	0.014	0.015
5721	320	400	450	490	-0.001	-0.002	-0.005
6087	310	380	430	450	-0.005	-0.008	-0.008
6300	260	320	350	370	-0.015	-0.022	-0.027
6312	280	330	350	360	0.006	0.008	0.010
6716	260	330	370	390	-0.018	-0.027	-0.035
6731	260	320	350	370	-0.008	-0.013	-0.017
7892	370	460	510	540	0.017	0.026	0.032
			MRK 533				
3727	550	700	800	880	0.017	0.029	0.043
3869	560	720	850	1350	0.025	0.060	0.205
4071	620	780	870	940	0.007	0.014	0.023
4363	540	700	820	930	-0.020	-0.066	-0.049
4686	850	1400	1580	1720	0.149	0.167	0.181
4861	420	560	820	930	0.039	0.156	0.173
4959	460	620	1030	1190	0.039	0.192	0.216
5007	460	610	970	1130	0.043	0.181	0.217
5119	420	520	570	610	-0.011	-0.018	-0.022
5305	470	590	660	710	-0.005	-0.009	-0.013
5721	620	950	1090	1160	-0.115	-0.139	-0.147
6087	1320	1770	1970	2300	0.082	0.102	0.145
6300	470	670	860	1160	-0.040	-0.048	-0.047
6716	450	620	760	880	-0.025	-0.045	-0.038
6731	410	560	690	780	-0.033	-0.067	-0.075
7135	460	590	670	730	0.001	0.002	0.003
7325	1220	1530	1700	1830	0.008	0.013	0.020
			MRK 704				
3426	710	900	990	1070	-0.004	-0.006	-0.010
3588	670	820	910	960	-0.001	-0.003	-0.006
3727	780	960	1060	1120	-0.009	-0.014	-0.015
3760	630	790	880	940	-0.016	-0.028	-0.037
3869	720	900	1000	1070	-0.001	-0.001	0.000
3893	720	1250	1420	1580	0.154	0.170	0.189
3968	700	860	950	1000	-0.005	-0.014	-0.016
4363	740	920	1020	1080	0.017	0.024	0.029
4868	590	770	900	1360	0.025	0.052	0.187
4861	570	720	810	870	0.031	0.046	0.057
4959	360	450	490	530	-0.012	-0.018	-0.022
5007	330	400	450	480	-0.004	-0.005	-0.007
5721	590	730	800	840	-0.003	-0.006	-0.007
6087	560	690	750	790	0.002	0.002	0.002
6375	730	900	990	1050	-0.001	-0.001	-0.002
6716	300	370	410	440	0.013	0.020	0.022
6731	340	430	490	540	-0.027	-0.048	-0.070
			MRK 975				
3426	930	1210	1400	1570	0.039	0.067	0.092
3727	470	590	650	700	-0.017	-0.027	-0.033
3760	920	1620	1730	1800	0.155	0.148	0.140
3869	870	1180	1560	1780	0.025	0.089	0.099
3968	930	1180	1320	1420	-0.023	-0.030	-0.031
4363	570	690	750	790	0.004	0.006	0.007
4959	580	810	1290	1420	0.051	0.189	0.196
5007	600	800	1100	1290	0.043	0.141	0.173
5721	660	820	920	990	-0.023	-0.033	-0.043
6087	1090	1850	2100	2240	0.151	0.162	0.160
6300	620	770	850	910	-0.001	-0.001	-0.002
6375	780	1050	2000	2070	-0.060	-0.251	-0.249
6716	340	440	510	610	0.015	0.036	0.040
6731	420	500	540	570	-0.020	-0.028	-0.032

TABLE 4—*Continued*

Lambda (Å)	$v_{1/2}$	$v_{1/3}$	$v_{1/4}$	$v_{1/5}$	$a_{1/3}$	$a_{1/4}$	$a_{1/5}$
			(km s^{-1})				
			MRK 1040				
3346	590	730	800	840	-0.002	-0.006	-0.006
3426	650	810	900	960	0.005	0.008	0.012
3727	590	720	790	830	0.011	0.014	0.014
3760	900	1100	1210	1280	-0.005	-0.006	-0.009
3869	550	690	750	800	0.025	0.034	0.038
4959	460	570	630	680	0.008	0.012	0.014
5007	490	600	670	710	0.007	0.015	0.020
5721	560	740	840	920	0.016	0.028	0.034
6087	630	850	950	1020	0.053	0.068	0.074
6300	320	400	440	470	0.017	0.022	0.026
6312	220	270	300	310	0.003	0.005	0.003
6375	620	850	940	1000	0.070	0.081	0.084
6716	310	390	430	460	0.021	0.034	0.043
6731	290	360	390	410	-0.011	-0.014	-0.017
			MRK 1126				
3426	320	390	430	450	0.012	0.016	0.017
3727	470	580	650	690	0.000	0.001	0.000
3869	340	420	470	500	0.008	0.012	0.015
4363	920	1150	1270	1360	-0.021	-0.035	-0.045
4686	390	490	530	560	-0.009	-0.012	-0.016
4861	180	230	260	270	-0.003	-0.003	-0.011
4959	210	270	300	340	0.036	0.061	0.084
5007	220	270	300	310	0.005	0.006	0.007
5199	310	370	400	430	-0.007	-0.008	-0.010
5721	410	500	550	590	-0.018	-0.027	-0.033
6087	520	650	730	790	-0.021	-0.037	-0.050
6300	370	450	490	510	0.003	0.004	0.005
6375	380	460	480	530	0.001	0.001	0.002
6716	320	390	430	460	0.008	0.013	0.014
6731	290	360	390	410	0.000	-0.001	-0.003
7135	300	380	420	450	-0.011	-0.018	-0.023
			MRK 1239				
3727	830	1020	1120	1190	-0.003	-0.006	-0.012
3760	1230	1550	1720	1840	-0.016	-0.030	-0.040
3840	1220	1510	1660	1790	-0.022	-0.034	-0.046
3869	960	1200	1330	1420	0.001	-0.001	-0.001
3893	910	1130	1240	1310	0.001	-0.002	-0.006
3968	830	1030	1130	1200	-0.008	-0.011	-0.015
4363	650	800	880	930	-0.004	-0.008	-0.011
4959	730	920	1030	1140	-0.009	-0.018	-0.029
5007	710	890	990	1070	0.008	0.017	0.027
5721	770	970	1070	1150	0.017	0.026	0.034
6087	1100	1880	2160	2340	0.150	0.168	0.178
6300	620	770	850	910	0.001	0.001	0.003
6375	760	990	1150	1280	0.039	0.067	0.087
6716	420	500	550	580	-0.005	-0.009	-0.011
6731	420	510	560	590	-0.006	-0.008	-0.011
			AKN 564				
3346	360	460	520	580	0.030	0.054	0.074
3426	370	460	500	540	0.015	0.025	0.030
3727	390	480	530	560	0.003	0.006	0.008
3760	630	830	1360	1410	0.045	0.200	0.199
3869	300	370	410	440	0.008	0.014	0.017
3893	860	1030	1120	1180	-0.025	-0.038	-0.047
3968	390	500	600	820	0.014	0.033	0.114
4363	500	640	760	880	0.034	0.068	0.111
4959	250	300	330	350	0.007	0.011	0.014
5007	240	300	330	350	0.007	0.011	0.014
5199	180	220	230	250	0.000	0.001	0.001
5721	340	420	470	510	-0.004	-0.007	-0.007
6087	480	620	710	780	-0.001	-0.004	-0.007
6300	260	320	360	380	-0.011	-0.021	-0.025
6375	660	830	920	980	0.013	0.019	0.022
6716	220	270	310	330	-0.017	-0.031	-0.047
6731	220	270	300	320	-0.015	-0.022	-0.030
7892	1210	1520	1700	1840	0.005	0.008	0.011

correlation in the data for NGC 4051. The formal relation, shown in Figure 4*c*, is

$$v_{1/3} = 0.2(\pm 1.0)\mathrm{IP} + 555(\pm 120)\,. \quad (8)$$

The most deviant point is the weak line [Ne v] λ3346. Ignoring this line does not significantly change the slope in the figure. A possible interpretation of this particular case will be mentioned later.

The highest ionization lines (of [Fe x], [Fe xi], and [Fe xiv]) have widths which are much larger than the low-ionization lines but are still substantially smaller than widths of the broad lines. But the ratios of the high- to low-ionization line widths, and of the broad-line to high-ionization line widths are comparable. It thus appears that there may not be a simple dichotomy between the broad-line region (BLR) and the NLR. Instead the continuum of widths suggests that there may be one volume filled inhomogeneously with clouds or filaments with a very wide range of density. In this picture the mean density and the velocity dispersion of the clouds decrease with distance from the photoionizing source, though not necessarily with the same scale lengths.

For some of the galaxies there is a definite correlation between the velocity in a line and the logarithm of the critical density of the level of the particular ionization state that emits the line. In particular (Fig. 5) for Mrk 9 and Mrk 975,

$$v_{1/3} = 252(\pm 83)\log_{10} N_{\mathrm{cr}} - 344(\pm 516) \quad (\mathrm{Mrk\ 9})\,,$$

$$v_{1/3} = 135(\pm 62)\log_{10} N_{\mathrm{cr}} + 175(\pm 394) \quad (\mathrm{Mrk\ 975})\,, \quad (9)$$

with correlation coefficients R of 0.6 and 0.7, respectively. Pelat, Alloin, and Fosbury (1981) for the Seyfert 1 NGC 3783, Atwood, Baldwin, and Carswell (1982) for NGC 3783 and Mrk 509, Cohen and Marcy (1983) for Mrk 704 and MCG 8-11-11, and Filippenko and Halpern (1984) for the "Liner" NGC 7213 have previously noted good correlations between line width and critical density for the narrow lines. For the galaxies we studied in which a formal correlation is noted, the slopes range from 21 to 252, and the differences are apparently real according to the formal errors quoted.

For the conceptual purposes we consider two extreme models consistent with this correlation: a "stratified" NLR in which the mean cloud density and velocity dispersion (and ionization state) is a monotonically decreasing function with distance from the photoionizing source, and a globally "unstratified" NLR in which clouds containing a wide range of densities (and ionization state) coexist throughout the entire NLR. In the stratified model (in which the clouds are assumed to be optically thin to the ionizing radiation) this correlation could suggest that the ionization zones are functions of distance from the ionizing source with "sharp" boundaries, if the velocity dispersion is also a well defined function of distance. Line emission will come primarily from these boundaries since collisional excitation is most efficient near the critical density. Pelat, Alloin, and Fosbury (1981) found that the high-ionization lines seem to come from smaller volumes compared with the low-ionization lines (although this conclusion may be somewhat model dependent) which may agree with the stratification hypothesis.

The "unstratified" model would suggest that the ionization boundaries are within the individual clouds. Thus low degrees of ionization could exist at essentially all radial distances, and high stages could exist over a wide range of distance, but on average closer to the central source than the low stages, and certainly not at the greatest distances. This could result if the narrow-line emission occurs in small clouds that are optically thick to ionizing radiation, so that although each cloud is stratified, even lines of low stages of ionization like [O i] and [S ii] can be emitted close to the central source of high-energy photons, as illustrated in Figure 1 of Osterbrock (1983).

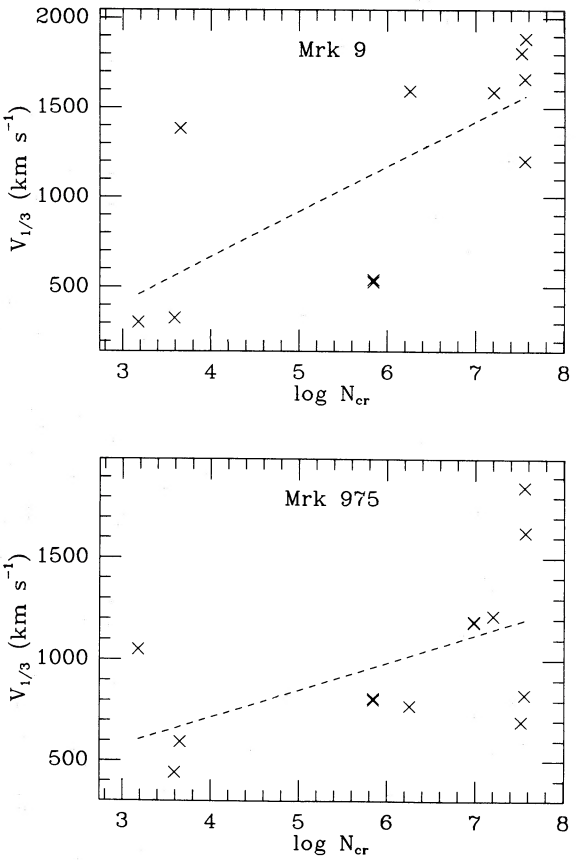

FIG. 5.—Correlations of emission-line widths (at one-third maximum intensity) with critical electron density (as defined in text) for two Seyfert 1 galaxies.

There is an excellent correlation between the asymmetry parameters at different relative intensities in each Seyfert galaxy. This is not surprising if profile asymmetry is intrinsic to the data and not generally the result of line blends, or the product of random error or numerical procedure. In particular, the relationship between the asymmetry at $\frac{1}{3}$ maximum, $a_{1/3}$, and $\frac{1}{5}$ maximum, $a_{1/5}$, is well fitted by

$$a_{1/3} = Ba_{1/5} + A\,, \quad (10)$$

where B ranges from 0.26 to 0.73, depending on the object, and A is always consistent with 0. Most of the objects have $B = 0.40$–0.60. In almost all cases the profiles are either skewed to the blue: NGC 4151 (slightly), Mrk 533, Mrk 975, Mrk 1040, and Akn 564; or are symmetric: NGC 4051, III Zw 77, Mrk 9, Mrk 359, Mrk 704, and Mrk 1239. Only 1126 may have marginally redward skewed narrow-line profiles. This is different from the situation for the broad H I line profiles, which when corrected for blending are skewed to the red, skewed to the blue, or approximately symmetric in about equal numbers of objects (Osterbrock and Shuder 1982; De Robertis 1984*a*). Figure 6 shows examples of the types of narrow-line symmetries encountered: Mrk 533 which has many more profiles

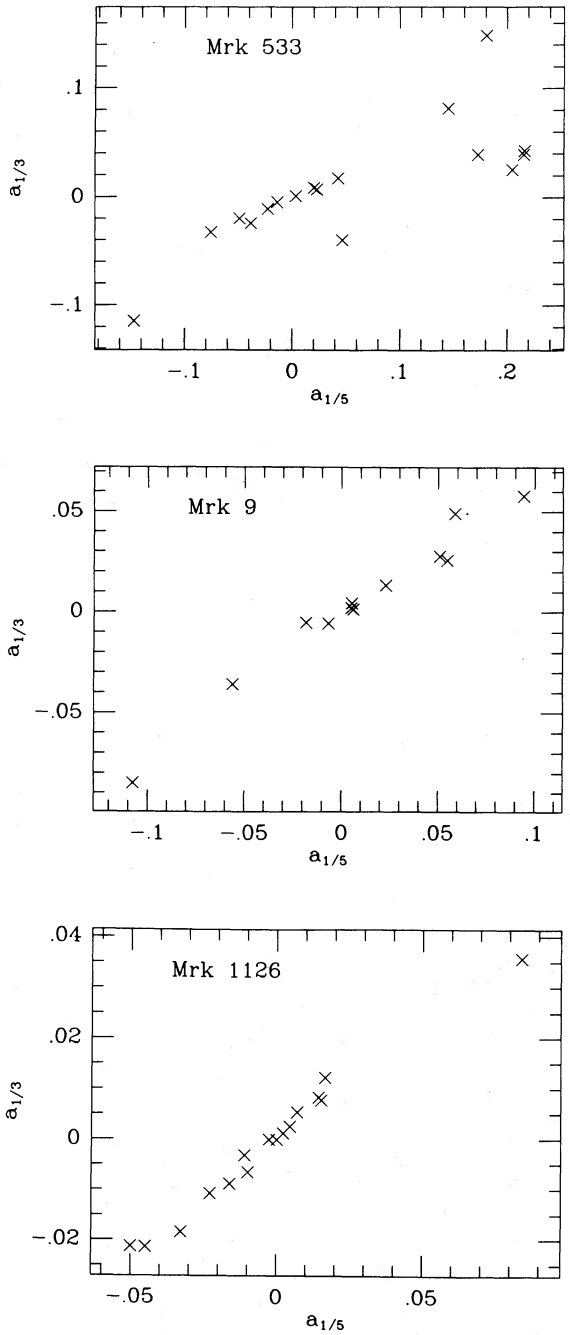

FIG. 6.—Correlations of asymmetry parameters (as defined in text) for three Seyfert galaxies

skewed to the blue, for Mrk 9 which has about equal numbers of lines skewed to the blue and red, and Mrk 1126 which is the only nucleus which shows more redward skewed lines than blue.

For all lines in a given object there is an excellent correlation between the widths of the lines at any two relative intensity levels. The relations between the widths at $\frac{1}{2}$ and $\frac{1}{4}$ maximum intensity, viz.,

$$v_{1/2} = Bv_{1/4} + A \,, \qquad (11)$$

have $R > 0.87$ for all objects. B ranges from 0.38 to 0.74, but almost all objects have B between 0.65 and 0.74 with a mean error for an individual object of ± 0.03. The constant A is almost always consistent with 0. Figure 7 shows examples for NGC 4151, Akn 564, III Zw 77, and Mrk 359. A correlation between widths is not unexpected. But the very small dispersion in slope for all objects is significant. (For comparison purposes, the slope for Gaussian profiles would be 0.71; for Lorentzian, 0.58; and for triangular, 0.67.) The ratios of widths at various relative intensities define the line profile and must ultimately be predicted by the proper geometry/acceleration mechanism for the NLR. It is interesting that De Robertis (1984*a*) has found, for the broad component of the Hβ profile in Seyfert 1 galaxies and QSOs, a similar excellent correlation. For 27 broad-line objects the analogous slope for the broad Hβ profiles was 0.63 (± 0.05): i.e., the same slope within errors. One interpretation of this similarity is that the same acceleration mechanism (and/or geometry) may be operating throughout both emitting-line regions.

II. There is good evidence that the absolute widths for some line correlate well with the absolute blue magnitudes as given in Table 3. It would presumably be most informative to compare line widths with the nuclear magnitudes alone, but this was not possible with the available data. The line widths for the low-ionization lines (e.g., [O I], [N I], or [S II]) tend to be correlated with the absolute magnitude of the total galaxy in the sense that brighter galaxies have broader lines. The line widths for the higher ionization lines (e.g., [Ne V] or [Fe VII]) do not show this correlation. Figure 8 shows one example for each case: [O I] + [N I] and [Ne V]. It is not clear how significant this trend with ionization potential is, but it may be related to the flux of ionizing radiation from the nucleus.

There is no correlation between the velocities in the narrow lines and the FWHM of the broad component of the Hβ line. This suggests but does not necessarily prove that the properties of the broad- and narrow-line regions are not coupled. There could be important geometrical differences between the regions which might make velocity comparisons difficult to interpret properly (e.g., Osterbrock 1979; De Robertis 1984*b*).

We considered in (I) the ratios of the line widths in a single object. Now for a given line in all galaxies an excellent correlation was also found between the widths at different relative intensities. The least-squares fits for most lines (except for [Fe VII]) for the analogous relation given by (11) yielded $R > 0.95$ with $B = 0.45$–0.74, with 0.66 as the mean. The mean slope may be only slightly different from that found in (I) according to the formal errors. It is not clear whether this is significant or not. Similar slopes in these two distinct cases may be an indication that the acceleration mechanism and/or geometry is the same in the narrow-line region for all Seyfert galaxies. The constant A is once again consistent with 0. Figure 9 shows this correlation for lines [N I] + [O I], [O III], [Ne V], and [Fe VII], respectively.

Finally, for a given line measured in all objects, there is an excellent correlation between the asymmetry parameters at different relative intensities. What may be of note is that the asymmetries of the lower ionization lines tend to be, on average, equally distributed about 0, whereas the high-ionization lines tend to have many more lines skewed to the blue. That is, [O I] + [N I], [S II], and [O II] have about equal numbers of profiles skewed to the red and the blue, while [O III], [Ne V], and [Fe VII] have a large percentage skewed to the blue. Figure 10 shows representatives from each category.

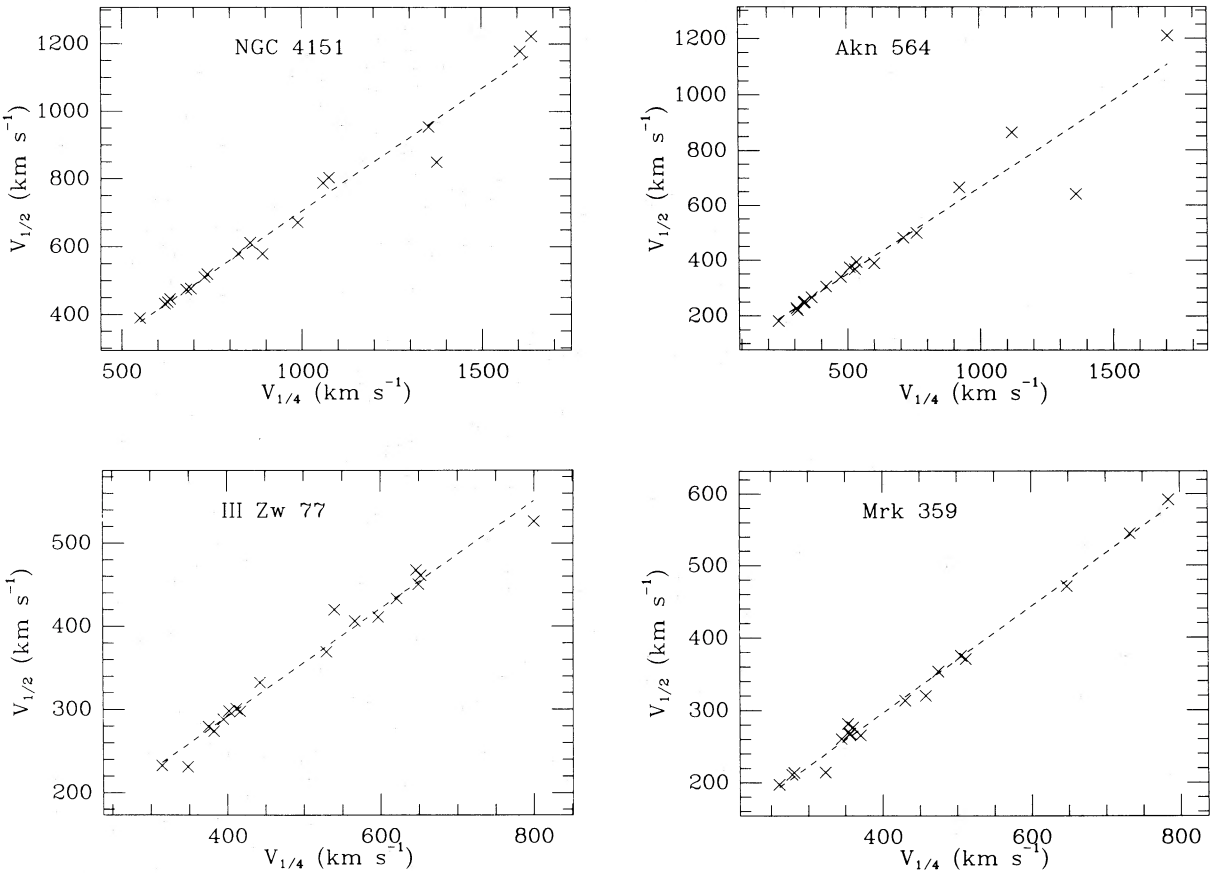

FIG. 7.—Correlations of emission-line widths at half and quarter maximum intensity for four Seyfert 1 and 1.5 galaxies

IV. DISCUSSION

a) Implications for the NLR

The characteristic FWHM of the narrow-lines in Table 4 is certainly greater than the central stellar velocity dispersion in typical galaxies. This argues against the emission-line gas being in gravitational equilibrium with the stellar mass distribution, as in orbital motion, unless the total mass is larger in active galactic nuclei than in "normal" ones. The preponderance of blue-wing excesses compared with the red in a large number of objects (see also Heckman *et al.* 1981; Whittle 1982; Vrtilek 1983) argues for radial motion for the narrow-line gas. The presence of reddening (see below) and of blue excesses suggests outward radial motion. As noted by Vrtilek (1983) orbital or random motion of the clouds would tend to produce a random distribution of asymmetries which is certainly not observed. Ballistic models requiring cloud production/acceleration at the central engine would have difficulty in explaining high-velocity clouds at distances ~ 100 pc from the source if there are in fact substantial drag effects produced by an interstellar or perhaps ambient medium. Radiative acceleration of gas clouds or filaments (e.g., Mathews 1974; Blumenthal and Mathews 1975) would, however, provide a natural explanation for the observed velocity fields. Clouds formed closer to the central source would be accelerated to larger absolute velocities than clouds formed further out which would lead to a stratified model for the NLR if the clouds are optically thin. Radiative acceleration could not only produce the remarkable similarity between profiles of all ionization states in a single object, but could also lead to the same profile variations between individual objects. If the broad-line profiles were also produced via radiative acceleration, then the apparent similarity between the broad Hβ and narrow-line profiles noted above could be understood.

The calculated lifetimes for the clouds to dissipate by expansion is much shorter than the characteristic time for crossing the narrow-line region. Thus if the clouds are not being continually generated within the region, they must be in some kind of pressure equilibrium with an assumed ambient medium (e.g., Mathews 1974; Krolik and Vrtilek 1984). According to this picture the pressure in the ambient medium is equal to the thermal pressure in the narrow-line clouds, $(nT)_A = (nT)_{\rm NLC}$. As noted earlier, $T_{\rm NLC} \approx 10^4$ K and $n_{\rm NLC} \approx 10^{3-6}$ cm^{-3}. Hence for $n_A \ll n_{\rm NLC}$, $T_A \gg T_{\rm NLC}$. A thermal wind in the Seyfert galaxy nucleus with $T \approx 10^{6-7}$ K might provide the confining pressure, or perhaps nonthermal pressures due to the observed radio-frequency emitting plasmas may confine the clouds, as suggested by Wilson and Willis (1980). If the density of the ambient medium decreases outward, and if the clouds are in pressure equilibrium with it, then the density of the clouds must also decrease outward.

These theoretical results, though mathematically correct, may be more simplified than the actual situation. The correlation of line width and critical density clearly shows that a very wide range of electron densities occurs in the NLR. A single representative electron density within the clouds is only the

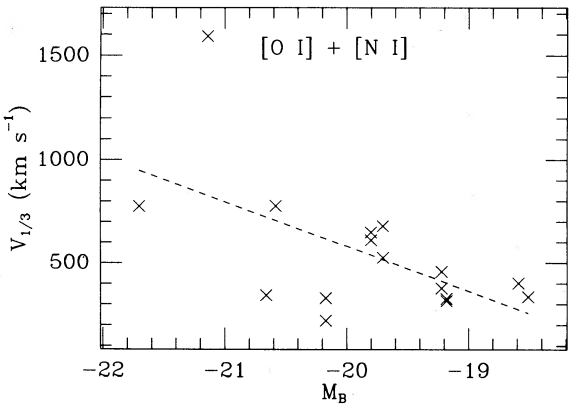

FIG. 8*a*

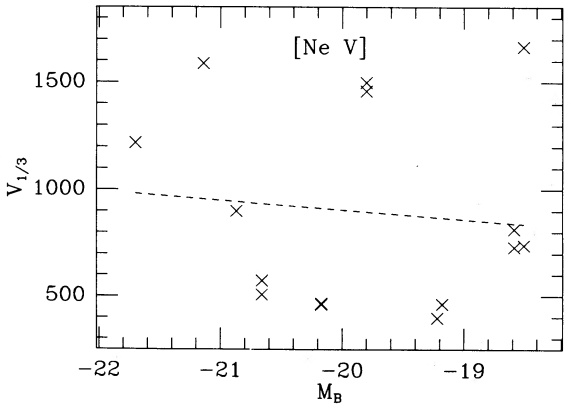

FIG. 8*b*

FIG. 8.—Correlations of emission-line widths at one-third maximum intensity of (*a*) [O I] λ6300 and [N I] λ5199, (*b*) [Ne V] λλ3426, 3346 with absolute blue magnitude for all the Seyfert galaxies of this paper.

coarsest possible description of the region. The separate correlation of ionization potential with line width shows that a wide range of densities occurs at each ionization level. Very probably the density and therefore pressure in each cloud are not exactly matched to the local pressure in the ambient medium, and therefore we are seeing clouds that are expanding and gas whose density is decreasing rapidly.

The wide range of line widths observed suggests that the division into a BLR region and a NLR is another extreme simplification. It seems quite possible that the BLR is the source of gas in the NLR, and the NLR, of the gas in the ambient region. If we adopt a typical BLR with a characteristic size $D \approx 10^{18}$ cm and a cloud velocity $v \approx 10^4$ km s^{-1} (Osterbrock 1978*b*), the characteristic time t is $t \approx D/v \approx 10^9$ s. Then if a typical BLR mass is $M \approx 10^2\ M_\odot$, the characteristic mass-loss rate is $M/t \approx 10^{-7}\ M_\odot$ s^{-1}. For a typical NLR we might take $D \approx 3 \times 10^{20}$ cm and $v \approx 3 \times 10^2$ km s^{-1}, yielding $t \approx 10^{13}$ s, and with $M \approx 10^7\ M_\odot$, $M/t \approx 10^{-6}\ M_\odot$ s^{-1}. All these values are so uncertain, and cover such a wide range in different objects, that these two mass gain (or loss) rates may be regarded as approximately equal.

The mass flow, arrangement of clouds, and other quantities may not be spherically symmetric. The physical situation may not be in a steady state. Clouds may form in ways we do not yet understand, as well as dissipate in ways we do not understand. Certainly dense neutral condensations survive for long periods of time in planetary nebulae, and constantly feed "new" ionized gas into the medium, far from its center (Capriotti, Cromwell, and Williams 1971). Perhaps the complicated actual structure seen in the best resolved direct photographs of NGC 1952, the Crab Nebula (e.g., Baade 1942; Trimble 1968), and NGC 7293, the Helix Nebula (e.g., Vorontsov-Velyaminov 1968), both of them examples of expanding flows, is more representative of the structure of NLRs than the idealized steady-state, spherically symmetric flow of the theoretical picture.

Reddening has been mentioned in the context of explaining the blueward asymmetries in the narrow lines (Heckman *et al.* 1981; Whittle 1982; Vrtilek 1983). The Balmer decrements in the narrow lines are steeper than expected from case B, suggesting that reddening is often important. A reasonable amount of intrinsic reddening can explain the observed ratios (e.g., see Costero and Osterbrock 1977). Does this extinction arise primarily in the narrow-line clouds or an ambient medium or both? There appears to be evidence for the last possibility. If the extinction were primarily from an ambient medium, then a stratified NLR would have more asymmetric, low-ionization lines and the unstratified model would show a blueward asymmetry, more or less the same for all lines. This is not observed. If the extinction were primarily from the clouds, it would be difficult to understand the predominance of blueward asymmetries in any model. Thus, there may be comparable amounts of reddening from both the clouds and an ambient medium.

b) Individual Objects

In order to isolate [O III] λ4363 and [Fe X] λ6375, Hγ λ4340 and [O I] λ6364 respectively had to be removed. The main concern with λ4363 is removing the broad component of Hγ λ4340. For this reason, the Hβ profile (always from the same spectral scan containing λλ4340, 4363) was scaled down to provide the best fit, shifted and subtracted as Hγ. (The same procedure was used to remove Hδ in a few instances.) The observed ratio of the fluxes in the broad Hγ to the broad Hβ varied between 0.30 and 0.38, which are less than the recombination value. Such deblends were considered to be acceptable when the mean level of the spectrum to the red of the G band and λ4363 was approximately at the adopted continuum value. When Hγ was removed via Hβ subtraction, in almost all cases there was an excess emission feature at about 4317(±5) Å. Identification of this feature is uncertain, although it is probably not Fe II judging from its relative strength with respect to known Fe II features in these objects. A possibility is [V X] $^3P_2$–$^1D_2$ λ4311.8, but the wavelength discrepancy seems a bit too large.

In the case of the [O I] λ6364 which contaminates [Fe X] λ6375, [O I] λ6300 was scaled by $\frac{1}{3}$, shifted to λ6364 and subtracted in much the same way as above.

In all but two objects, [O III] λ4363 was (usually considerably) broader than [O III] λλ4959, 5007. Filippenko and Halpern (1984) also found differences in profile widths between lines from the same stage of ionization as in this case. They argue that this might result if clouds spanning a large range in density occupy the same general volume about the photoionizing source. In our spectra [Ne V] λ3346 was broader than [Ne V] λ3426 in all but two instances. This is probably the result of blending with O III λ3341, a Bowen resonance-fluorescence line, and/or [Ne III] λ3342. In a few objects noted below, [Ne V] λ3426 appeared to have an associated broad

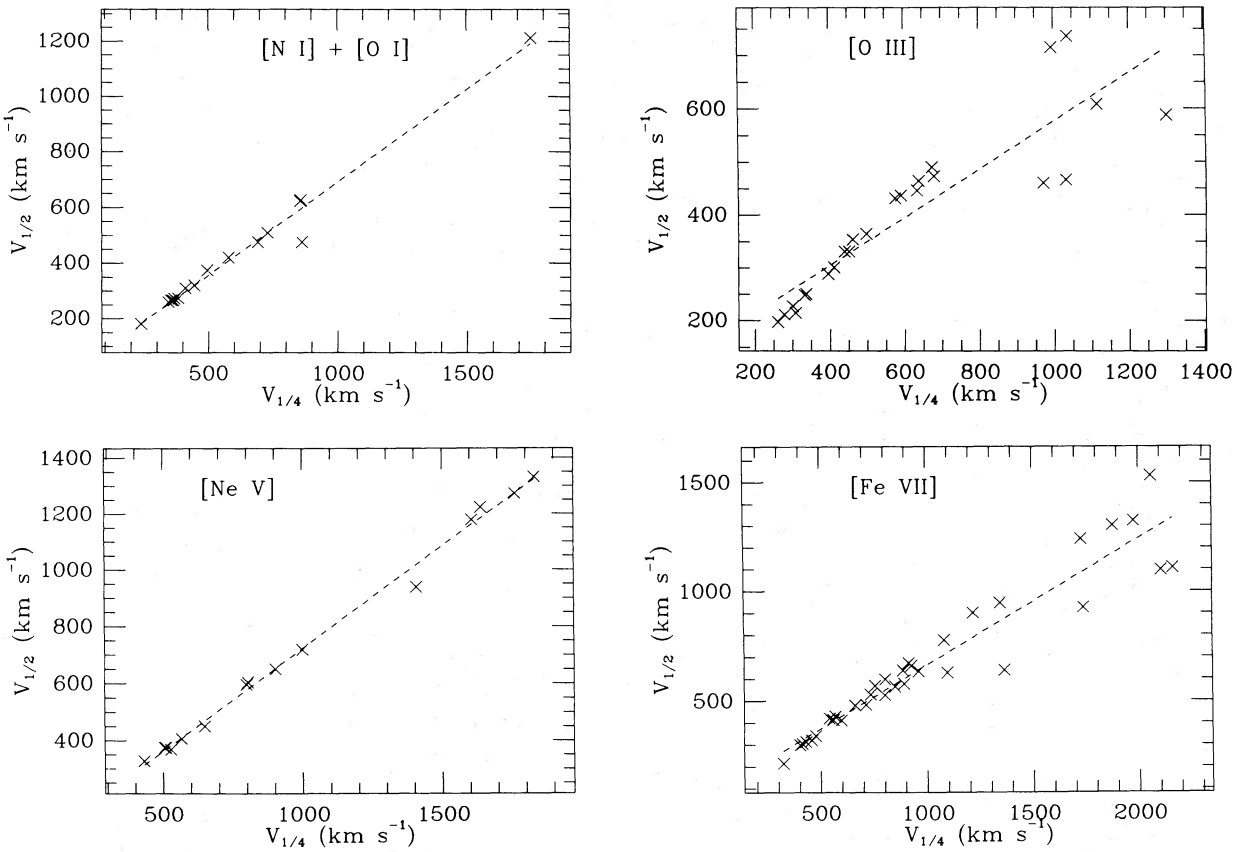

FIG. 9.—Correlations of emission-line widths at one-half and one-fourth maximum intensity, for all the Seyfert galaxies of this paper

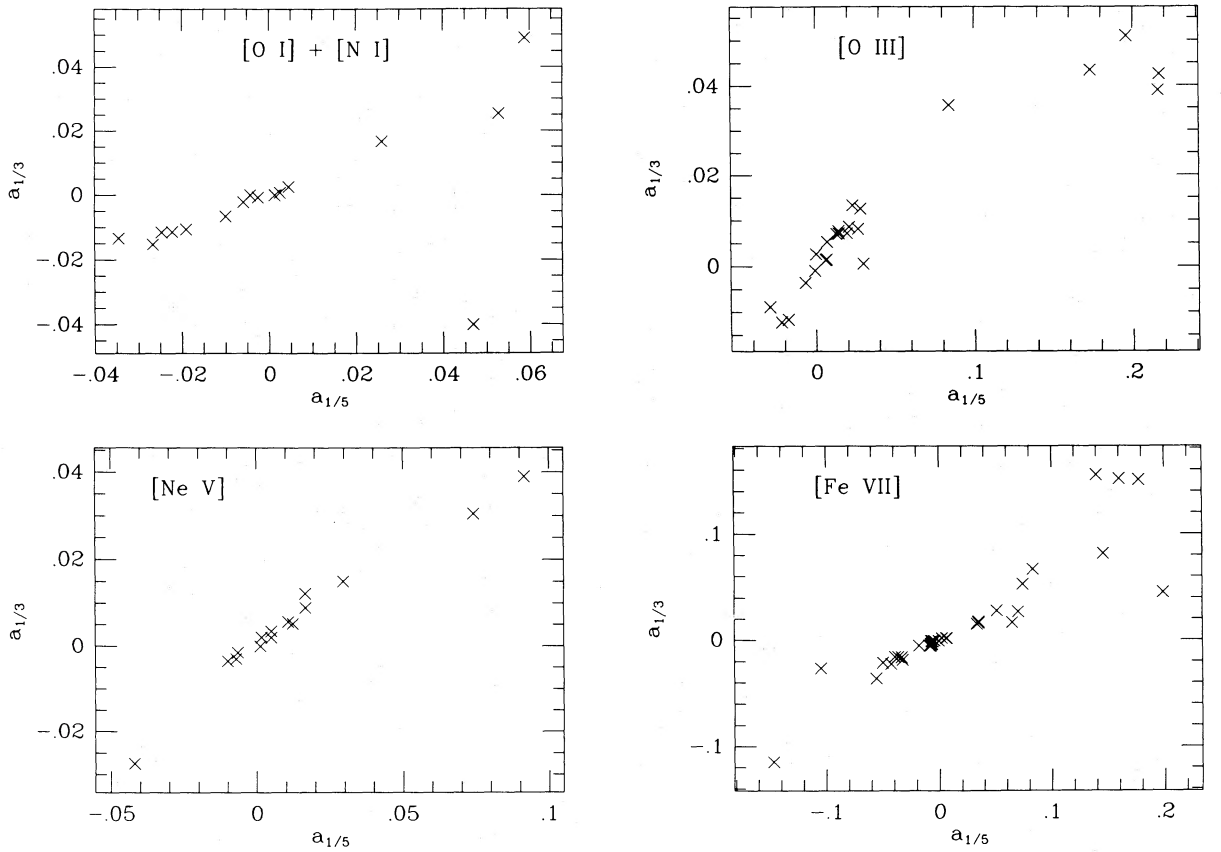

FIG. 10.—Correlations of asymmetry parameters (as defined in text) for the emission lines shown, in all the Seyfert galaxies of this paper

base, while in scans of similar signal-to-noise of other objects, no base was present.

The following is a summary of distinctive trends or features that were noticed in the optical spectrum during the analysis. In general the Hγ subtraction proved acceptable unless otherwise noted. Also [S II] λλ6716, 6731 had very similar profiles with the exceptions mentioned below.

NGC 4051.—The most noticeable feature of the spectrum is that the ratio of the high-ionization line widths (especially [Fe VII]) to the low-ionization widths is considerably smaller than in other objects in this sample. Figure 4*c* shows this phenomenon.

[Ne V] λ3346 is very broad and asymmetric compared with λ3426. [N I] λ5199 is blended with another feature about 8 Å to the blue of line center. There is evidence for [S III] λ6312 emission in the red wing of [O I] λ6300. The red wing of [Fe X] λ6375 appears to be blended. It was difficult to properly fit a continuum for [Fe XI] λ7892.

NGC 4151.—These emission lines are relatively broad, compared with the narrow lines of the other galaxies included in this paper. There is some excess red extension to [Ne V] λ3426. There are emission features in both wings of λ3727 and λ3967. The presence of [S II] λ4068 is apparent after Hδ subtraction. There appear to be broad features in both wings of λ6087. [O I] λ6300 is relatively strong and broad with some red excess (probably [S III] λ6312).

III Zw 77.—Strong high-ionization emission lines characterize the spectrum of this object (Osterbrock 1981). There appears to be a possible broad base to the [Ne V] λ3426. It may be up to 150 Å wide at zero intensity. [Fe VII] λ3588 may be blended in the red wing. Hγ subtraction proceeded well, although the narrow component of Hγ appeared to exceed the scaled Hβ profile. There is a definite emission feature at about 4317 Å in the blue wing of Hγ. There is a noticeable blue excess in the λλ4959, 5007 lines. The [S II] lines have a slight red excess. The continuum placement for [Fe XI] λ7892 is highly uncertain.

Mrk 9.—There is rather strong Fe II present in the optical spectrum in this object. Following the method of De Robertis (1984*a*) we find that the equivalent widths of λλ4924, 5018 of multiplet (42) are about 15% that of broad Hβ. The broad permitted lines make continuum fitting difficult.

There appears to be an extended red wing to [Ne V] λ3426. [O II] λ3727 seems to be centered on an Fe II swell, and is extended noticeably to the blue. Although it is difficult to subtract Hγ from λ4363, the latter is unquestionably broader than λ5007. [O III] λλ4959, 5007 are noticeably extended to the blue. Of the [Fe VII] lines, λ5721 has a red blend and λ6087 seems to be blended in the blue wing. [O I] λ6300 appears to be very broad. We suggest that it is blended with a strong line in the blue, since the profile is much more highly skewed to the blue than any other line. Both [S II] lines appear to have secondary maxima on the blue wing. There is probably a strong blend in the wing of [Fe XI] λ7892.

Mrk 359.—The lines are somewhat narrow and symmetric in this object. [Ne V] λ3346 is skewed to the blue and is noticeably broader than λ3426. [O III] λ4959 shows a slight redward asymmetry (perhaps a blend) compared with λ5007. There are some continuum placement problems for [Fe VII] λ5156, [Fe VI] λ5176, and [N I] λ5199. There is strong [S III] λ6312 emission.

Mrk 533.—Essentially all lines appear to be highly extended to the blue. The identification of [Fe V] λ4071 is tentative because of the Hδ subtraction. [O III] λ4363 is redward asymmetric, perhaps due in part to the Hγ subtraction. There is a definite excess in the blue wing of Hγ at about 4320 Å. [N I] λ5199 is significantly affected by broad Mg I *b* absorption. It is difficult to measure [Fe VII] λλ5721, 6087 because of potential blending in the wings. The [S II] λλ6717, 6731 profiles are similar.

Mrk 704.—Although [Ne V] λ3426 emission is strong, there is little λ3346 present in the ultraviolet scan. The subtraction of Hγ gave only poor results for [O III] λ4363. A strong λ4317 feature was present in the blue wing of Hγ. There appeared to be strong absorption on the blue side of He II λ4686, which makes the narrow He II component difficult to isolate. There is a noticeable emission feature at about λ6106 in the red wing of λ5087. [O I] λ6300 appears to be weak, and there may be a strong [S III] λ6312 component. The [S II] lines only marginally have the same profile.

Mrk 975.—In general the profiles for this object show a blueward excess. Possibly there is some Fe II emission in the optical spectrum. [Ne V] λ3346 appears much broader (and noisier) than λ3426. The latter appears to have a broad base. [Ne III] λ3869 appears blended in the blue wing, and in the red by [Fe V] λ3896. Also [Ne III] λ3968 may be blended. The λλ4959, 5007 lines are highly skewed to the blue at the base. Almost certainly, there is a blend in the blue wing of λ6087, and blue and red blends in [Fe X] λ6375. Although there may be some Hα contamination, the [S II] λλ6716, 6731 profiles are the most dissimilar of any one object. They differ in both width and asymmetry.

Mrk 1040.—In general, lines are skewed to the blue in this object. This is the only object in which [Ne V] λ3346 appears to be narrower than [Ne V] λ3426, although λ3426 appears to have a blend in the blue wing. It was not possible to subtract Hγ by scaling the Hβ profile. Either the two Balmer profiles are markedly different in this object, or there are enough emission line blends near Hγ to confuse the situation. There is measurable [S III] λ6312 emission. The [Fe X] emission line, while strong, is centered at λ6367.

Mrk 1126.—The narrow emission-lines are very narrow in this object. There is a small redward asymmetric trend in many of the line profiles. While Hγ subtraction proved acceptable, the narrow component of the scaled Hβ profile was considerably stronger than the actual Hγ. A small blue excess is evident at the bases of λλ4959, 5007. The [S II] line profiles are less similar in this galaxy than in most of the others.

Mrk 1239.—This scan has the poorest signal-to-noise ratio in the continuum in the sample. There appears to be a red excess (blend?) in the wing of [Fe VII] λ3760. There is almost certainly blending in [Ne III] λ3869. This is the only galaxy in the sample in which the [Fe X] λ3840 profile could be measured. Unfortunately, the scatter in the relation between line width and critical density is fairly large in this object, so the estimated [Fe V] critical density cannot be tested by these data. Mrk 1239 is one of two galaxies in the sample in which [O III] λ4363 is narrower than λλ4959, 5007. There are almost certainly blends in the blue wing of λ6087. [Fe X] λ6375 has a very large blue excess as well. Because of proximity of broad Hα emission and the atmospheric B band, the continuum fitting was slightly uncertain for the [S II] lines.

Akn 564.—The general level of ionization appears to be nearly as high as in III Zw 77. However, there is weak Fe II emission, which makes certain identification of [Fe XIV] λ5303 difficult if not impossible. There seems to be a blue excess in

λ3346. There is some evidence for a broad base in λ3426. (There is a strong feature at λ3453 which might contribute to this.) [Fe VII] λ3760 has strong blends in the wings, especially the blue. [Ne III] λ3968 has a much broader base than λ3869. While the Hγ subtraction is acceptable, there is a strong emission line between Hγ and λ4363. [O III] λ5007 is contaminated by Fe II λ5018 and was not measured, since λ4959 is so strong. [Fe VII] λ6087 is strong but seems to have a different profile from λ5721. There is obvious [S III] λ6312 emission in the red wing of [O I] λ6300. [Fe X] emission is strong with a noticeable blue excess. There appears to be a slight red excess in the bases of the [S II] lines.

V. SUMMARY

Profiles have been measured for a large number of narrow emission lines, covering a wide range of ionization potential and critical densities for de-excitation in 12 Seyfert 1 and 1.5 galaxies. These emission-line profiles show a wide variety of widths and asymmetries. In each galaxy, however, the profiles are similar in form, though differing in scale. There is a good correlation between line width and ionization potential in many of these galaxies, and also a correlation between line width and critical density for some of the objects. This must imply not only that all the observed stages of ionization are present, but also that a wide range of densities, up to at least the highest critical electron densities that fit the correlation, $N_{cr} \sim 10^{7-8}$ cm^{-3}, must be present in the "narrow-line" region. These profile measurements thus confirm that in many Seyfert 1 and 1.5 galaxies there must be a broad range of density, extending more or less continuously from the "broad-line region" through the "narrow-line region." The relative velocity widths of a given line (such as [Fe VII] λ6087) at corresponding fractions of maximum intensity are very nearly the same in all the galaxies.

The narrow-line profiles are mostly either asymmetric in the sense of being skewed to the blue, or are symmetric. The asymmetry is consistent with radial outflow or expansion of the gas, together with extinction by dust. The widths of the high-ionization lines (or high critical-density lines) are correlated with the absolute magnitudes of the nucleus, indicating that radiation pressure may be important, but the same correlation does not extend to the low-ionization (or low critical-density) lines.

The average form of the narrow-line profiles, expressed in dimensionless terms, is quite similar to the average form of the broad-line profiles in Seyfert 1 and 1.5 galaxies (neglecting asymmetry effects) determined by De Robertis (1984*a*). This may imply that the same acceleration mechanism is operative in both, leading to velocity fields with similar overall structure. The continuity of densities of course adds weight to this idea. However, the fact that the broad-line and narrow-line widths are not well correlated, and that the broad-line profiles have little if any preferred asymmetry while the narrow-line profiles are almost all either symmetric or skewed to the blue, is not easy to interpret in this picture.

We are grateful to J. M. Shuder, R. D. Cohen, and O. Dahari for their assistance in obtaining the data that went into this paper, and to them and to W. G. Mathews, J. S. Miller, and M. Whittle for many stimulating discussions of line profiles and velocity fields in active galactic nuclei. We are also grateful to the National Science Foundation for support of this research under grants AST 79-19227 and 83-11585.

REFERENCES

Atwood, B., Baldwin, J. A., and Carswell, R. F. 1982, *Ap. J.*, **257**, 559.
Baade, W. 1942, *Ap. J.*, **92**, 188.
Bowen, I. S. 1960, *Ap. J.*, **132**, 1.
Brault, J. W., and White, O. R. 1971, *Astr. Ap.*, **13**, 169.
Blumenthal, G. R., and Mathews, W. G. 1975, *Ap. J.*, **198**, 517.
Capriotti, E. C., Cromwell, R. H., and Williams, R. E. 1971, *Ap. Letters*, **7**, 241.
Cohen, R. D., and Marcy, G. W. 1983, *Bull. AAS*, **15**, 654.
Costero, R., and Osterbrock, D. E. 1977, *Ap. J.*, **200**, 675.
Davidson, K., and Netzer, H. 1979, *Rev. Mod. Phys.*, **51**, 715.
De Robertis, M. 1984*a*, *Ap. J.*, submitted.
———. 1984*b*, in preparation.
Filippenko, A. V., and Halpern, J. P. 1984, *Ap. J.*, **286**, in press.
Garstang, R. H. 1957, *M.N.R.A.S.*, **117**, 393.
Heckman, T., Miley, G., van Breugel, W., and Butcher, H. 1981, *Ap. J.*, **247**, 403.
Huchra, J. P. 1983, "Seyfert Data," private communication.
Krolik, J. H., and Vrtilek, J. M. 1984 C.F.A. preprint.
Mathews, W. G. 1974, *Ap. J.*, **189**, 23.
Mendoza, C. 1983, in *IAU Symposium 103, Planetary Nebulae*, ed. D. R. Flower (Dordrecht: Reidel), p. 143.
Miller, J. S., Robinson, L. B., and Schmidt, G. D. 1980, *Pub. A.S.P.*, **92**, 702.
Miller, J. S., Robinson, L. B., and Wampler, E. J. 1976, *Advances in Electronics and Electron Physics* (New York: Academic Press), Vol. **40B**, p. 693.
Nussbaumer, H., and Storey, P. J. 1978, *Astr. Ap.*, **70**, 37.
———. 1982, *Astr. Ap.*, **113**, 21.
Osterbrock, D. E. 1978*a*, *Phys. Scripta*, **17**, 285.
———. 1978*b*, *Proc. Nat. Acad. Sci.*, **75**, 540.
———. 1979, *A. J.*, **84**, 901.
———. 1981, *Ap. J.*, **246**, 696.
———. 1983, in *IAU Symposium 103, Planetary Nebulae*, ed. D. R. Flower (Dordrecht: Reidel), p. 473.
Osterbrock, D. E., and Shuder, J. M. 1982, *Ap. J. Suppl.*, **49**, 149.
Pelat, D., Alloin, D., and Fosbury, R. A. E. 1981, *M.N.R.A.S.*, **195**, 787.
Pritchet, C., Mochnacki, S., and Yang, S. 1982, *Pub. A. S. P.*, **94**, 733.
Robinson, L. B., and Wampler, E. J. 1972, *Pub. A. S. P.*, **84**, 161.
Shuder, J. M., and Osterbrock, D. E. 1981, *Ap. J.*, **250**, 55.
Trimble, V. 1968, *A. J.*, **73**, 535.
Vorontsov-Velyaminov, B. A. 1968, in *IAU Symposium 34, Planetary Nebulae*, ed. D. E. Osterbrock and C. R. O'Dell (Dordrecht: Reidel), p. 256.
Vrtilek, J. M. 1983, unpublished Ph.D., Harvard University.
Walker, M. F. 1968, *Ap. J. (Letters)*, **154**, L53.
Whittle, M. 1982, *Pub. A.S.P.*, **94**, 760 (see also unpublished Ph.D. thesis, Cambridge University).
Wilson, A. S. 1979, *Proc. Roy. Soc. London, A*, **366**, 461.
Wilson, A. S., and Willis, A. 1980, *Ap. J.*, **240**, 429.

Note added in proof.—Two lines of the data in Table 4 for III Zw 77 are incorrect, and the following two lines should be substituted for them:

6300	280	350	390	425	−0.014	−0.025	−0.035
6375	370	470	530	585	−0.013	−0.023	−0.034

M. M. De Robertis and D. E. Osterbrock: Lick Observatory, Board of Studies in Astronomy and Astrophysics, University of California, Santa Cruz, CA 95064